ELSEVIER

Chemical Physics 234 (1998) 1–19

Chemical Physics

Intramolecular proton transfer in the ground and the two lowest-lying singlet excited states of 1-amino-3-propenal and related species [1]

Marta Forés, Miquel Duran, Miquel Solà *

Institut de Química Computacional and Departament de Química, Universitat de Girona, 17071 Girona, Catalonia, Spain

Received 27 January 1998

Abstract

The potential energy surfaces of the ground state and the two lowest-lying singlet excited states of 1-amino-3-propenal, the cyclic complex of 1-amino-3-propenal with water, and salicylaldimine (2-iminomethylphenol) have been investigated theoretically along the proton transfer (PT) reaction coordinate. All these three systems have in common the same intramolecular H-bond through an OCCCN backbone. It has been found that the PT in the $\pi\pi^*$ excited state of 1-amino-3-propenal has a very small energy barrier, which disappears after introduction of dynamic correlation, providing a pathway for an ultrafast photoinduced PT. The energy barriers for the PT processes of the ground and $n\pi^*$ states increase when the transfer of the proton is carried out through a water molecule bridge. Calculations reveal two main differences between 1-amino-3-propenal and salicylaldimine: (a) while in 1-amino-3-propenal the keto tautomer is the most stable in all the electronic states studied, the ground state of salicylaldimine favors the enol structure; (b) the near degeneracy between the $n\pi^*$ and $\pi\pi^*$ excited singlet states in 1-amino-3-propenal is lost in salicylaldimine, for which the $\pi\pi^*$ excited singlet state is stabilized as compared to the $n\pi^*$ state. These results suggest that care must be taken in generalizing to larger molecules the conclusions obtained with models as small as 1-amino-3-propenal.

1. Introduction

The photoinduced excited-state intramolecular proton transfer (ESIPT) process is one of the most fundamental photochemical reactions, which has been studied both experimentally (see Refs. [1–3] for recent reviews) and theoretically [4–18] for many years. It is well established that the proton transfer (PT) in most systems takes place very rapidly in the excited states [3] as a consequence of a drastic change in the acidity and basicity of the proton donor and acceptor groups in the molecule after the electronic excitation [3,19–24]. The ESIPT reaction is usually followed by a large red-shifted fluorescence of the phototautomer (6000–10000 cm^{-1}) [3,25].

It is also known that some compounds that present ESIPT processes are ultraviolet absorbers because of the presence of chromophores like C=O, C=N, N=O or C=C. The study of the emission and

* Corresponding author. E-mail: miquel@iqc.udg.es

[1] This paper is dedicated to Albert, son of M. Solà, born during the elaboration of this paper.

0301-0104/98/$19.00
PII: S0301-0104(98)00165-7

absorption spectra of these compounds has proved that some of them are photostable in the excited states. This property allows their use as photoprotecting agents [26,27] and triplet quenchers [28]. It has also been successfully demonstrated that several dyes showing ESIPT are efficient lasing materials [29,30]. Also, these compounds may have the appropriated characteristics to be used as molecular switches in hypothetical logic or memory circuits [31], provided that one can guarantee the photostability of the phototautomer in the excited state.

The derivatives of benzotriazole [32–34], 2,5-bis-(2-benzoxazolyl) hydroquinone [35], *N*-phenylanthranilic acid [36], *N*-salicylidene [25,37–39], 2-(2′-hydroxyphenyl) benzimidazole [40–42], 2-(3′-hydroxy-2′-pyridyl) benzimidazole [43] 2-(2′-hydroxyphenyl) oxazole [17] and 2-(2′-hydroxyphenyl) benzoxazole [44,45] have been extensively studied experimentally, in part because these molecules present ESIPT reactions and can be potentially useful in the development of lasers, photostabilisers and information storage devices. From a theoretical point of view, their study is limited to semi-empirical methods due to the size of the molecules. It is usual to take only a subset of their molecular structure, which contains the atoms involved most in the intramolecular H-bond, and to study theoretically their ESIPT processes by more reliable methods. This can be, in part, justified by experimental work suggesting that the PT reactivity and photochromism are strongly localized in a definite small fragment of the absorbing system and that molecules with the same chromophore yield similar UV/VIS spectra [25]. The smallest model system containing the essential atoms involved in the PT of the aforementioned compounds is 1-amino-3-propenal. The PT of this system in the ground state and the two first singlet excited states has already been studied at the CASSCF and MRCI levels of theory [46].

Our aim is to extend this previous work to larger compounds which are structurally closer to the molecules studied experimentally. For this reason, our study is performed using the computationally less expensive CIS and CIS-MP2//CIS methodologies with three main purposes. First, to compare the results yielded by both methodologies with those obtained at the CASSCF and MRCI levels for 1-amino-3-propenal in order to check whether these methodologies can reproduce, at least qualitatively, the results furnished by the CASSCF and MRCI levels of theory. Second, it is well known that the ESIPT processes in solution are rather sensitive to solvent effects [1,2,36,45,47–50]. Thus, the influence of solvation on the relative stabilities of the tautomers and on the energy barriers along the PT reaction coordinate are estimated by introducing explicitly a water molecule in our model system. Finally, salicylaldimine (2-iminomethylphenol), a more conjugated system which is structurally closer to the molecules experimentally studied, is analyzed and the results obtained are compared to those of the 1-amino-3-propenal model system and also to those obtained from experimental studies on molecules with similar structure. In that way we expect to gain insight on the effect of conjugation which has already been found to be essential in ESIPT reactions [51].

2. Computational details

All calculations have been performed by means of the GAUSSIAN 94 package [52]. The molecular geometries of all molecular systems studied in this work have been optimized at the restricted Hartree–Fock (RHF) level for the ground state, whereas the configuration interaction all single-excitations method (CIS) [53] with a spin–RHF reference ground state has been employed to make full and constrained optimizations in the excited states. We have also performed single point energy calculations for the ground and excited states using the second-order perturbation correction MP2 and CIS–MP2 [53] methodologies (MP2//HF and CIS–MP2//CIS), respectively. For similar systems to those studied here, it has been found that inclusion of polarization functions into the basis set is essential to obtain the correct ordering of the lowest excited singlet states [54] while diffuse functions have little effect on the results [13,55]. For this reason, the double-zeta gaussian basis set of Dunning and Hay with polarization functions (D95**) [56] has been used throughout.

Quantum molecular similarity measures (QMSM) and euclidean distances [57–67] have been obtained from the GAUSSIAN-94 generalized electron densi-

ties [68,69] using the MESSEM program [70,71]. In this work, the definition of QMSM between densities $\rho_I(\mathbf{r})$ and $\rho_J(\mathbf{r})$ is given by [57,58]:

$$\mathbf{Z}_{IJ} \int \rho_I(\mathbf{r})\, \rho_J(\mathbf{r})\, \mathrm{d}\mathbf{r} \qquad (1)$$

while the euclidean distance between these two electron densities is obtained as [57,58]:

$$d_{IJ} = [\, Z_{II} + Z_{JJ} - 2 Z_{IJ}\,]^{1/2} \qquad (2)$$

From the definition of Eq. (2) it is found that a zero distance means that electron densities $\rho_I(\mathbf{r})$ and $\rho_J(\mathbf{r})$ are exactly the same, whereas a large value of the distance implies the existence of significant differences between the two electron density distributions.

3. Results and discussion

3.1. 1-Amino-3-propenal system

Most geometry optimizations of the excited states of 1-amino-3-propenal have been performed under C_S symmetry, the molecules being kept planar unless explicitly specified otherwise. The lowest-lying singlet excited states of all systems considered in this work result from $n\pi^*$ and $\pi\pi^*$ excitations, which have the symmetry representations A″ and A′, respectively, in the C_S point group. The two tautomers of 1-amino-3-propenal, which are planar in the ground state, lose their planarity in the excited states when they are fully optimized with the CIS method, and the two almost degenerate lowest-lying excited states mix together. It is nearly impossible to get a converged solution for the highest of the two close-lying excited states with the same multiplicity and symmetry; on the contrary, under C_S symmetry it is easy to converge both states because they belong to different symmetry representations. For this reason most theoretical studies on ESIPT maintain the systems planar in the excited states [5–9,17,46,54]. It is expected that distortions from the C_S symmetry will have a negligible effect when the excited state presents a nearly barrierless PT. In that case an ultrafast ESIPT will occur before the relaxation of the originally planar geometry, since out of plane vibrational motion takes longer than an ultrafast PT event, which occurs in the femtosecond time range [3,17,72]

Moreover, it has been shown for malonaldehyde [13] and 1,5-diaza-1,3-pentadiene [73] that electronic correlation acts to favor the planar geometry in the excited states. This notwithstanding, the influence of permitting full distortion upon the energetics of the ESIPT reactions of 1-amino-3-propenal have also been analyzed and compared to the results obtained for the C_S constrained ESIPT processes. Unfortunately, in this case it has not been possible to locate the enol tautomer and the transition state (TS) of the ESIPT reaction for the highest of the two close-lying excited $n\pi^*$ and $\pi\pi^*$ states, because they lie too close to the conical intersection, and the orbital mixing in this region are extensive enough to prevent the location of the two excited forms.

All located TSs exhibit the expected normal imaginary frequency with a transition vector that corresponds to the motion of the atoms during the PT process. Due to the preference for nonplanar structures, the excited-state planar TSs exhibit an additional imaginary frequency for a mode breaking the C_S symmetry.

The optimized main geometrical parameters of the two tautomeric forms (see Fig. 1) and the TSs for the PT processes in the ground and the two lowest-lying excited states under C_S symmetry are reported in Table 1. Considering a simple Lewis structure, the keto form has two double bonds ($C_4=O_5$ and $C_2=C_3$), whereas these bonds in the enol tautomer become simple bonds, the double bonds being $N_1=C_2$ and $C_3=C_4$. The bond lengths in Table 1 illustrate this variation when going from the keto to the enol tautomer. The formally double bonds elongate and the single bonds shorten by nearly 0.1 Å. All the optimized parameters of the TS range be-

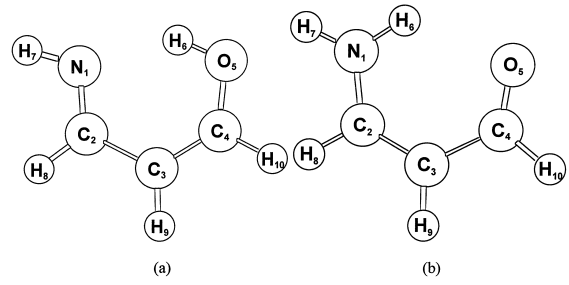

Fig. 1. The ground state optimized geometries of the (a) enol and (b) keto tautomers of 1-amino-3-propenal.

Table 1
Most relevant optimized geometrical parameters (Å and degrees) of the two tautomeric forms of 1-amino-3-propenal and the transition state that connects the two tautomers

	$r(N_1–C_2)$	$r(C_2–C_3)$	$r(C_3–C_4)$	$r(C_4–O_5)$	$r(N_1–H_6)$	$r(O_5–H_6)$	$r(N_1–O_5)$	$\theta(N_1–H_6–O_5)$
enol								
S_0	1.271	1.461	1.344	1.318	1.884	0.961	2.701	141.2
$n\pi^*$	1.318	1.448	1.338	1.354	2.303	0.943	3.040	134.5
$\pi\pi^*$	1.337	1.407	1.447	1.297	1.698	0.996	2.584	146.0
TS								
S_0	1.296	1.419	1.385	1.269	1.261	1.186	2.370	151.1
$n\pi^*$	1.280	1.385	1.374	1.271	1.222	1.124	2.243	146.0
$\pi\pi^*$	1.304	1.418	1.457	1.256	1.368	1.124	2.423	152.9
keto								
S_0	1.342	1.359	1.451	1.210	0.997	2.089	2.778	124.5
$n\pi^*$	1.372	1.343	1.463	1.265	0.991	2.328	2.940	119.1
$\pi\pi^*$	1.338	1.450	1.433	1.248	1.012	1.902	2.707	134.2

tween those of the enol and keto tautomers, with the only exception of the $r(N_1–O_5)$ distance and the $\theta(N_1–H_6–O_5)$ angle which take the shortest and the largest values, respectively, in the TS of each state. This is not surprising because in the TS the H_6 atom is shared by the N_1 and O_5 atoms, and so in this molecular structure these two atoms have to be close each other. Interestingly, it has been shown recently that the in-plane deformation vibrational mode that modulates the separation between the proton donor and acceptor atoms plays an important role in the ESIPT processes, by opening a barrierless channel for the PT in the excited state potential energy surface [3,72,74]. The short $N_1–O_5$ bond length of our optimized TSs compared to the values of the same bond distance in the two tautomers reflects the importance of this vibrational mode in the dynamics of the ESIPT processes.

A qualitative molecular orbital representation of the highest occupied molecular orbital (HOMO), the second highest occupied molecular orbital (SHOMO), and the lowest unoccupied molecular orbital (LUMO) is shown in Fig. 2 for the enol and keto tautomers. The HOMO and LUMO have π symmetry while the SHOMO is of σ type. The two excited states are mainly the result (other contributions are not significant) of transferring an electron from the SHOMO to the LUMO ($n\pi^*$ excited state with A'' symmetry), and from the HOMO to the LUMO ($\pi\pi^*$ excited state with A' symmetry). The $\pi\pi^*$ excited state has significant oscillator strength, while the oscillator strength of the $n\pi^*$ excited state is very small. The nature of the molecular orbitals help us to understand the changes in the bond lengths after promoting the molecule to the excited states. For instance, for the enol form, whereas the electronic contribution between C_2 and C_3 atoms in the HOMO orbital is antibonding in the LUMO orbital is bonding, and as a consequence, the $r(C_2–C_3)$ bond distance is shortened in the $\pi\pi^*$ excitation by 0.054 Å. Similarly, the $r(C_3–C_4)$ bond distance is lengthened by 0.103 Å in the same transition because the C_3 and C_4 atoms in the HOMO orbital are connected by a bonding contribution while the interaction between these two atoms in the LUMO orbital is antibonding.

The $r(N_1–H_6)$ bond distance in the enol form can be taken as a measure of the H-bond strength. This bond distance in the $\pi\pi^*$ state is clearly shorter than in the other states, which means that, among the electronic states analyzed, the strongest intramolecular interaction between N_1 and H_6 atoms is found for this state. On the contrary, the $r(N_1–H_6)$ bond distance of the enol tautomer in the $n\pi^*$ state is the largest one, indicating that the enol tautomer forms the weakest H-bond in the $n\pi^*$ state. This conclusion is also supported by the $r(O_5–H_6)$ bond distance and the $\theta(N_1–H_6–O_5)$ angle: the enol tautomer of the $\pi\pi^*$ state has the largest $r(O_5–H_6)$ bond distance and $\theta(N_1–H_6–O_5)$ angle.

The relation established above between the H-bond strength and the geometrical parameters is consistent with the adiabatic Mulliken charges (Table 2)

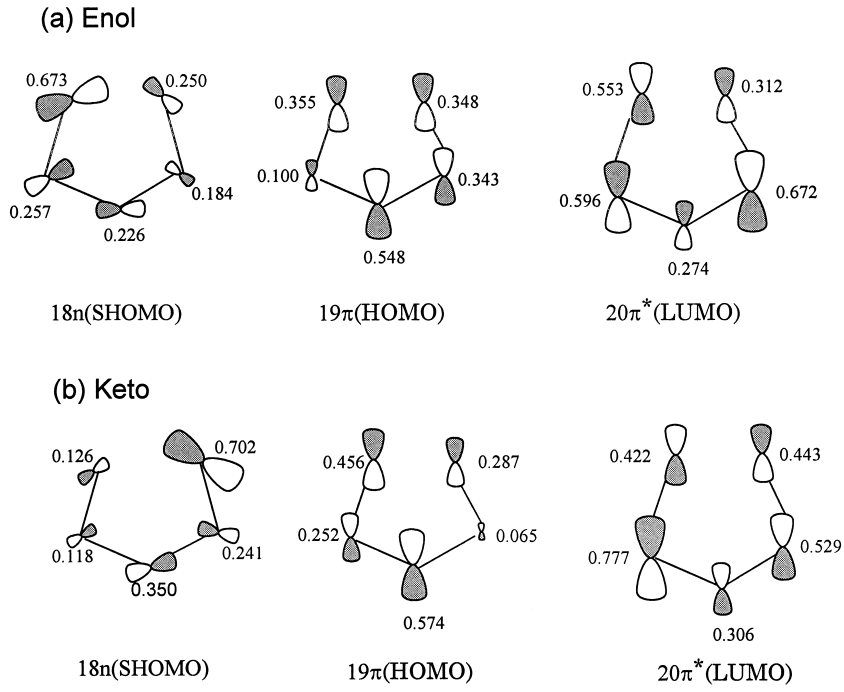

Fig. 2. Schematic diagram of the orbital structure of the SHOMO, HOMO, and LUMO for the (a) enol and (b) keto tautomers of 1-amino-3-propenal. The numbers correspond to the value of the molecular orbital coefficient obtained from the square root of the sum of the squared coefficients of intervening atomic orbitals.

obtained from the relaxed geometry of the excited states. Since the nature of the H-bond is mainly electrostatic, it is expected that a large positive charge in H_6 and negative charge in the proton acceptor group will lead to stronger H-bonds. Indeed, the $\pi\pi^*$ state of the enol form has the H_6 with the highest positive charge and N_1 with the most negative charge among the three states analyzed. Similar arguments taking into account the $r(O_5–H_6)$ bond distance and Mulliken atomic charge population lead to the conclusion that in the keto form the strongest H-bond is also found for the $\pi\pi^*$ state and the weakest corresponds to the $n\pi^*$ state. Similar results were obtained by Luth and Scheiner for glyoxalmonohydrazine [55], in which the two tautomers show also the strongest H-bond for the $\pi\pi^*$ singlet excited state.

Table 2
Vertical and adiabatic Mulliken atomic charge populations (au) of the atoms most involved in the proton transfer

	q_v(O)	q_v(N)	q_v(H_6)	q_a(O)	q_a(N)	q_a(H_6)
enol						
S_0	−0.463	−0.527	0.411	−0.463	−0.527	0.411
$n\pi^*$	−0.453	−0.199	0.417	−0.485	−0.132	0.386
$\pi\pi^*$	−0.375	−0.524	0.399	−0.345	−0.538	0.432
keto						
S_0	−0.442	−0.551	0.347	−0.442	−0.551	0.347
$n\pi^*$	0.018	−0.580	0.350	0.045	−0.596	0.340
$\pi\pi^*$	−0.445	−0.397	0.341	−0.467	−0.433	0.364

Let us now discuss what happens to the charge density distribution of the two tautomers when an electron is promoted to the π^* orbital. Fig. 3 plots the density differences for the enol and keto forms between the ground and the $n\pi^*$ and $\pi\pi^*$ excited states at the ground state optimized geometries. The most important effect in the $n\pi^*$ transition is a reduction of charge in the basic group of each tautomer, as one can expect because in this transition an electron is promoted from an orbital located mostly on oxygen in the keto form and on nitrogen in the enol form to a delocalized π^* orbital. This variation is depicted in Fig. 3, where the solid lines indicate a loss of the electronic density going from the ground

to the excited states. Solid lines are denser in the basic atom of each tautomer. These atoms are less basic in the $n\pi^*$ state than in the ground state, so they cannot attract H_6 as strongly as they do in the ground state and the H-bond becomes weaker in this excited state. The changes observed in the electronic distribution upon excitation to the $n\pi^*$ state are also reflected by the vertical Mulliken charge populations gathered in Table 2.

When an electron is transferred from the π to the π^* orbital the most important change is located in the π system of the carbon atoms, as one can expect from the coefficients of the molecular orbitals in Fig. 2. However, there is also some loss of charge in the acidic groups of each form, which is difficult to see in the density difference plots due to the mix of positive and negative differences around these atoms, but can be deduced from the vertical Mulliken atomic charge populations. The reduction of negative charge in the acidic group is consistent with an increase of the H-bond strength after $\pi\pi^*$ photoexcitation.

Although the density difference plots provide information only in the selected plane of representation, they already seem to indicate that the $n\pi^*$ transition undergoes a greater variation in the electronic density distribution than the $\pi\pi^*$ transition. In order to confirm this conclusion, QMSM and euclidean distances between S_0, $\pi\pi^*$, and $n\pi^*$ electron density distributions computed at the ground state geometry are gathered in Table 3. A previous work [75] has shown that the self-similarity value, i.e. the QMSM when $\rho_I(\mathbf{r})$ and $\rho_J(\mathbf{r})$ are the same electron densities, is a measure of the degree of charge density concentration: the greater the self-similarity, the more concentrated the electronic density. According to Table 3, the ground and $\pi\pi^*$ states have a similar charge density concentration, while the charge density in the $n\pi^*$ state is less concentrated. This is not at all surprising, since when an electron is promoted from an n to a π^* orbital, the electronic charge goes from a localized orbital to a more delocalized orbital, and hence the charge density in the $n\pi^*$ state is somewhat more diffuse, thus yielding a decreased self-similarity value. Furthermore, euclidean distances in Table 3 give a quantitative measure of the importance of the change in the electron density distribution after photoexcitation. It is found that the largest difference appears in the $n\pi^*$ transition, as already predicted by the density difference plots. Interestingly, the large change in the electron density observed in the $n\pi^*$ state does not translate into larger geometrical changes for this state. The nuclear rearrangement is more important for the $\pi\pi^*$ excitation, as a result of the 19π HOMO and the $20\pi^*$ LUMO having an almost opposite nodal structure.

Table 4 collects the energy difference (ΔE) between the two tautomers (positive values indicate that the keto form is more stable than the enol form) and the energy barriers of the PT that transforms the enol to the keto tautomer ($\Delta E_d^{\ddagger}$) and the keto to the enol form ($\Delta E_r^{\ddagger}$). The keto tautomer is more stable than the enol tautomer in all the three states studied at all levels of theory. HF/CIS and MP2/CIS–MP2//HF/CIS yield the same ordering in the ΔE values among the three states analyzed as CASSCF [46] ($\Delta E^*_{n\pi} > \Delta E^*_{\pi\pi} > \Delta E_{So}$). Upon inspection of the $\Delta E_d^{\ddagger}$ values computed at HF/CIS levels one can notice that the two tautomeric forms are separated by each other through a relatively high barrier in the ground and the $n\pi^*$ states, whereas the barrier for the $\pi\pi^*$ state is rather small. Similar results were obtained for *o*-hydroxybenzaldehyde [11] and for 2-(2′-hydroxyphenyl) benzoxazole [8] using the CASSCF and CIS methods, respectively, and also for the same 1-amino-3-propenal at the CASSCF level [46]. It is worth noting that in the CASSCF study [46] the potential energy surfaces (PES) of the excited states were calculated at the optimized geometry of the ground state. According to this work [46] the PT in the $\pi\pi^*$ state is barrierless while the ground and $n\pi^*$ states have significant barriers. Not surprisingly, the inclusion of dynamic correlation by means of the MP2/CIS–MP2//HF/CIS method

Fig. 3. Plot of density differences between S_0–$n\pi^*$ and S_0–$\pi\pi^*$ for the enol and the keto forms of 1-amino-3-propenal in a plane 0.4 Å above and parallel to the molecular plane: (a) S_0–$n\pi^*$ in enol; (b) S_0–$\pi\pi^*$ in enol; (c) S_0–$n\pi^*$ in keto, and (d) S_0–$\pi\pi^*$ in keto tautomers. The minimum contour is $1 \times 10 - 3$ au and they increase to 2, 4, 8, 20, 40, 80, $\ldots \times 10^{-3}$ au. Dashed lines correspond to negative values, that is, points where the excited state has greater density than the ground state.

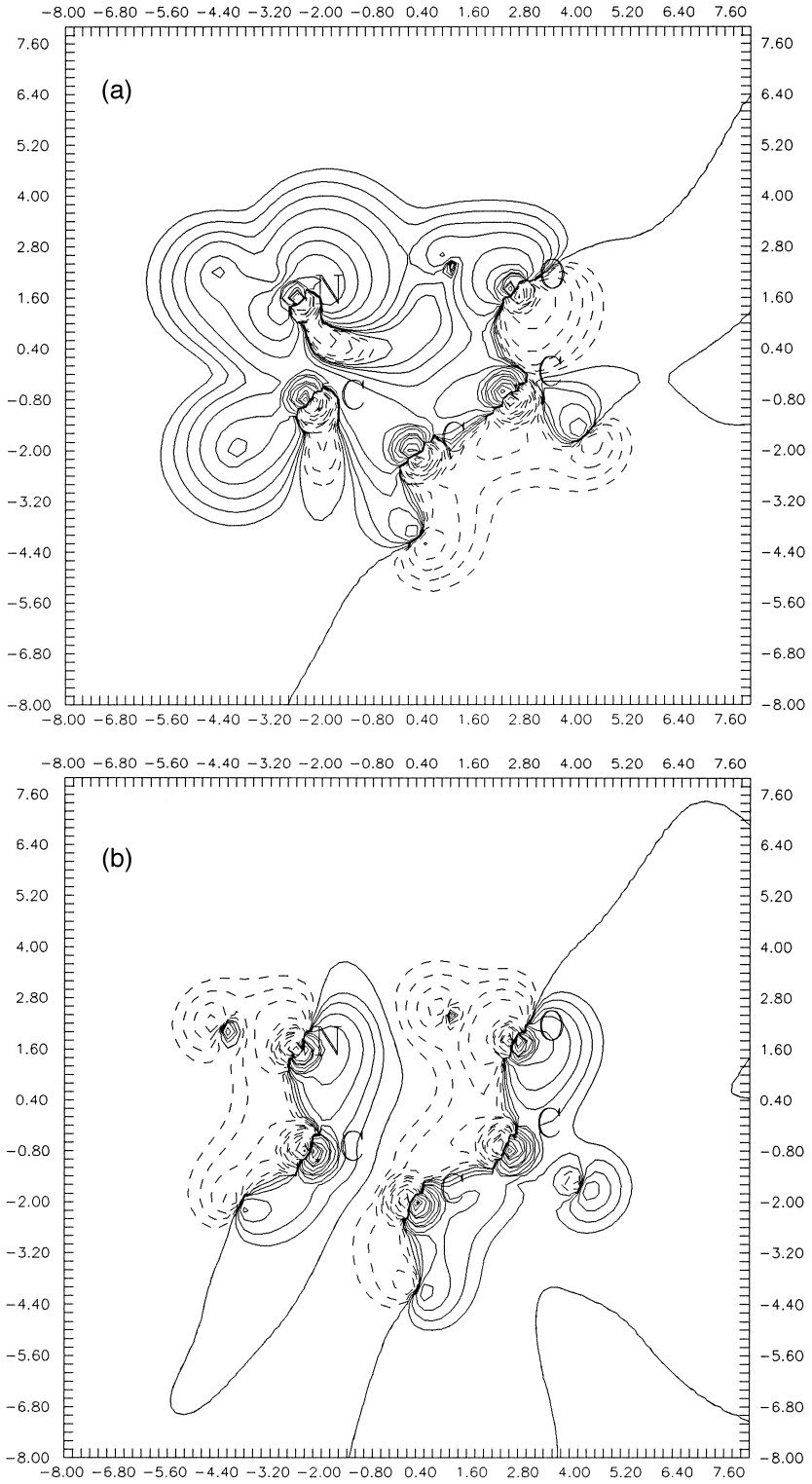
(a)
(b)
−8.00 −6.80 −5.60 −4.40 −3.20 −2.00 −0.80 0.40 1.60 2.80 4.00 5.20 6.40 7.60
7.60 6.40 5.20 4.00 2.80 1.60 0.40 −0.80 −2.00 −3.20 −4.40 −5.60 −6.80 −8.00

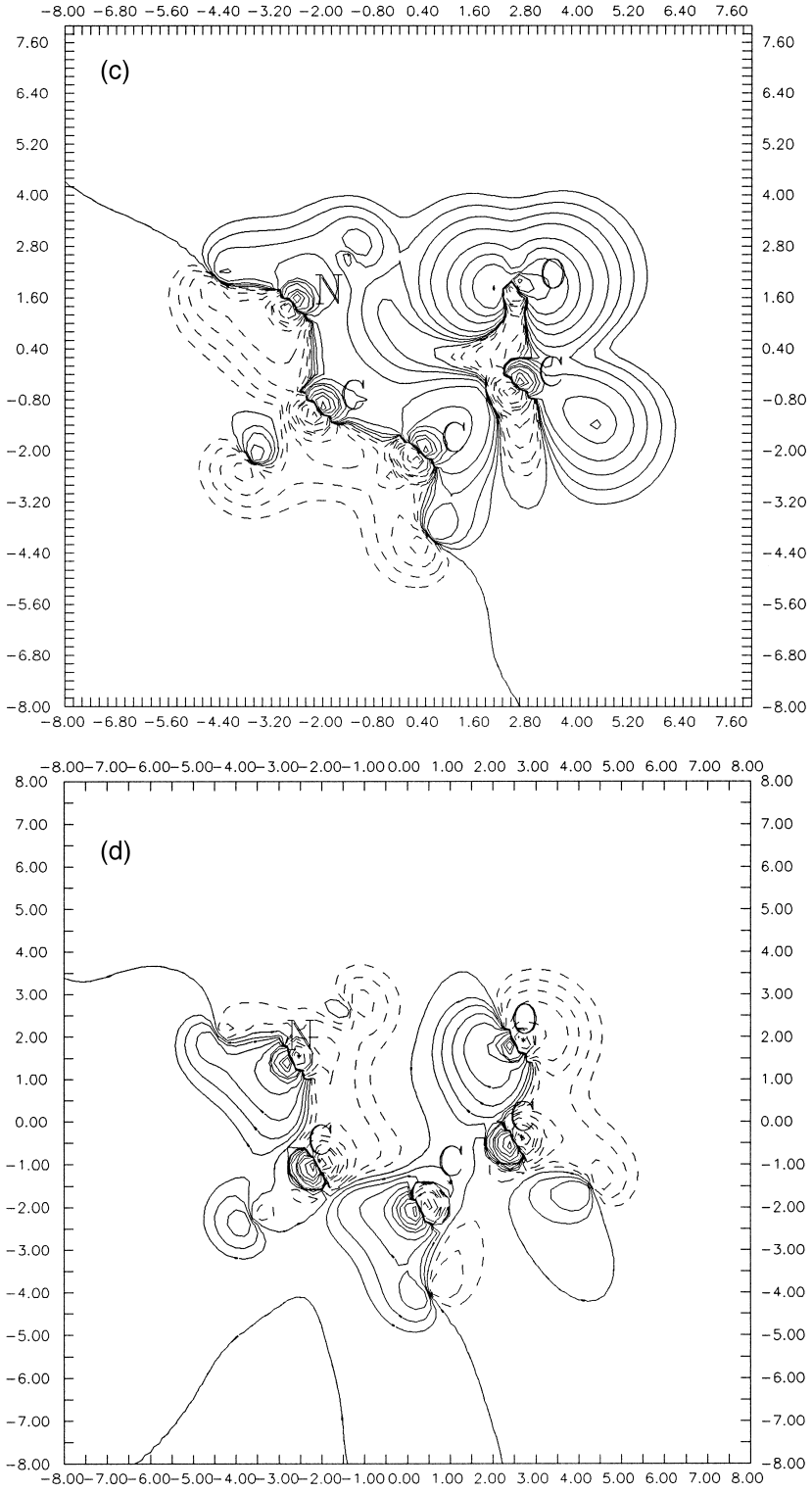

Fig. 3 (continued).

Table 3
Quantum molecular similarity measures and euclidian distances (in italics) between electron density distributions of the electronic states studied for the two tautomers of 1-amino-3-propenal

	S_0 [a]	$n\pi^*$ [a]	$\pi\pi^*$ [a]
enol			
S_0	228.619	*0.203*	*0.077*
$n\pi^*$	228.535	228.491	*0.196*
$\pi\pi^*$	228.621	228.541	228.630
keto			
S_0	228.553	*0.261*	*0.087*
$n\pi^*$	228.506	228.527	*0.249*
$\pi\pi^*$	228.555	228.515	228.565

[a] au.

reduces drastically the energy barriers. At the CIS–MP2//CIS level the small barrier predicted by the CIS method for the PT in the $\pi\pi^*$ state disappears in agreement with the results obtained at the CASSCF level [46]. Thus, the small barrier for the PT found by the CIS methodology in the $\pi\pi^*$ state can be attributed to the lack of correlation energy when using the CIS method. Moreover, the elimination of the energy barrier for the PT in the $n\pi^*$ state and the drastic reduction of the barrier in the ground state at the MP2/MP2–CIS//HF/CIS level are probably due to the well-known fact that MP2 overestimates the correlation energy [10,13,17,73,76,77]. In fact, the CASSCF results predict meaningful barriers for the PT in the So and $n\pi^*$ states of 1-amino-3-propenal [46]. Preliminary results for 1-amino-3-propenal with the CASPT2 method also indicate that the ground and $n\pi^*$ states show significant barriers, despite these barriers being lower than those predicted by CIS [78]. Further, it was found that CASSCF yields a notable barrier for the PT of the *o*-hydroxybenzaldehyde in the $n\pi^*$ state [11], which is not removed after introduction of dynamic correlation. All these results lead to the conclusion that in most cases CIS overestimates the energy barriers for the PT processes while CIS–MP2 underestimates them. As a whole, all levels of theory predict that after electronic excitation of the enol form to the $\pi\pi^*$ state an ultrafast PT from the oxygen to the nitrogen atom will take place if the molecule follows the diabatic curve.

Table 4
Energy difference (ΔE) between the two tautomeric forms of 1-amino-3-propenal and direct ($\Delta E_d^{\ddagger}$) and reverse ($\Delta E_r^{\ddagger}$) energy barriers for the proton transfer that transforms the enol to the keto form computed at the HF/CIS and MP2/CIS-MP2//HF/CIS (in italics) level

	ΔE [a]	$\Delta E_d^{\ddagger}$ [a]	$\Delta E_r^{\ddagger}$ a
S_0	8.7 (15.4/19.8)[b]	8.7	17.4
	7.1	*0.6*	*7.6*
$n\pi^*$	16.4 (29.6/32.7)[b]	26.7	43.1
	26.2	*− 1.6*	*24.5*
$\pi\pi^*$	9.0 (17.3/39.5)[b]	3.5	12.5
	13.8	*− 4.6*	*9.3*

[a] kcal/mol.
[b] Values in brackets are CASSCF/MRCI results from Ref. [46].

The HF/CIS energy profiles of the PT reaction along the reaction coordinate (taken as the difference between $r(N_1–H_6)$ and $r(H_6–O_5)$) are represented in Fig. 4 for the ground and the $n\pi^*$ and $\pi\pi^*$

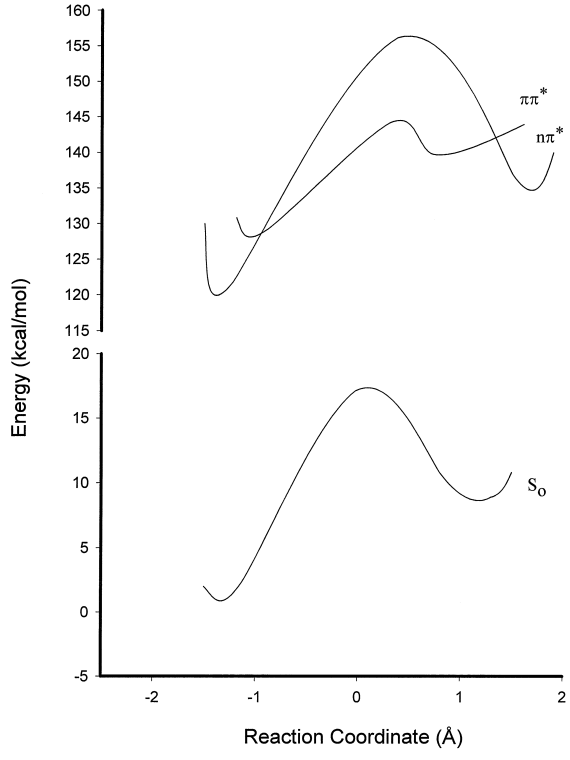

Fig. 4. Energy profiles for the proton transfer in the ground and excited states of 1-amino-3-propenal obtained by full geometry optimization in the ground state and imposing C_S symmetry in the geometry optimizations of the excited states. The reaction coordinate corresponds to the difference between $N_1–H_6$ and $H_6–O_5$ bond lengths. The zero energy value is taken as the energy of the keto tautomer in the ground state.

states. It is interesting to note the double crossing between the $n\pi^*$ and $\pi\pi^*$ states along the reaction coordinate, which can be responsible for a nonreactive process in the $\pi\pi^*$ state if the molecule crosses the states, as suggested by Sobolewski and Domcke [46]. Therefore, the conical intersection [79] between the $n\pi^*$ and $\pi\pi^*$ states may play an important role in the photochemical reactivity because the crossing in the PES may compete with the PT process, thus opening a channel for inhibition of the ESIPT process and giving photostability to the enol tautomer. Our calculations at the CIS level indicate that, if the ESIPT process takes place, the system will eventually yield a 6600 cm^{-1} red-shifted fluorescence of the ESIPT process in the keto form [46].

As far as the influence of full optimization upon the energetics of the ESIPT is concerned, it is found that the enol tautomer in the $\pi\pi^*$ state is much more stabilized by the geometrical relaxation (34.6 kcal/mol) than the keto tautomer (1.2 kcal/mol), which has approximately the same energy as in the planar geometry. This is reinforced by a greater structural change in the enol form than in the keto form. Whereas the keto form remains practically planar, the enol tautomer suffers an important structural distortion which can be explained by the electronic change that takes place in each transition. Similar results were reported by Luth and Scheiner for the same transition in glyoxalmonohydrazine [55] a molecule that has a structure similar to 1-amino-3-propenal. In the $\pi\pi^*$ transition, an electron goes to the π^* orbital, so the molecule loses partially the double π bond character and it is more free to rotate. The enol form changes the C_2–C_3–C_4–O_5 dihedral angle from 0° to −88.7° and the C_2–C_3–C_4–H_{10} dihedral angle from 0° to 89.9°. The fact that the enol form is more stabilized than the keto form at the relaxed geometry leads to a switch in the relative stabilities of two tautomers in the $\pi\pi^*$ state. In this state, the enol form is favored over the keto form by 25.6 kcal/mol. The high stabilization of the enol tautomer in the $\pi\pi^*$ is also reflected by the direct energy barrier, which increases to 29.3 kcal/mol. The distortion that undergoes the enol form in this state breaks the H-bond and consequently the ESIPT reaction becomes more difficult. However, as we have pointed out, the PT is faster than the out of plane deformation vibrational motion, and so it is expected that after photoexcitation from the planar ground state to the $\pi\pi^*$ state, an ultrafast ESIPT will take place before the relaxation of the molecular geometry may occur. As mentioned above, it has not been possible to locate the unconstrained enol form and TS for the $n\pi^*$ transition.

3.2. Complex of 1-amino-3-propenal with water

The HF/D95** optimized geometries of the two tautomeric forms of the complex of 1-amino-3-propenal with water in the ground state are depicted in Fig. 5, while the most important geometrical parameters of the tautomers and the TS that connects them for the three states analyzed are summarized in Table 5. As one can see from Fig. 5, the complex forms a double H-bond between the water molecule and the acid and basic groups of 1-amino-3-propenal. Thus, in this case the PT occurs through a biprotonic transfer, i.e. a proton is transferred from the proton donor atom to the water molecule and from the water molecule to the proton acceptor atom of 1-amino-3-propenal. Both the keto and the enol forms are nonplanar in the ground state. Remarkably, the ground state nonplanar keto structure of Fig. 5b is favored over a planar structure by only 0.3 kcal/mol. Moreover, a planar enol conformer 3.5 kcal/mol more stable than the nonplanar enol complex of Fig. 5a has been located in the PES of the ground state. Its geometrical parameters have also been gathered in Table 5. In this planar conformer, the original

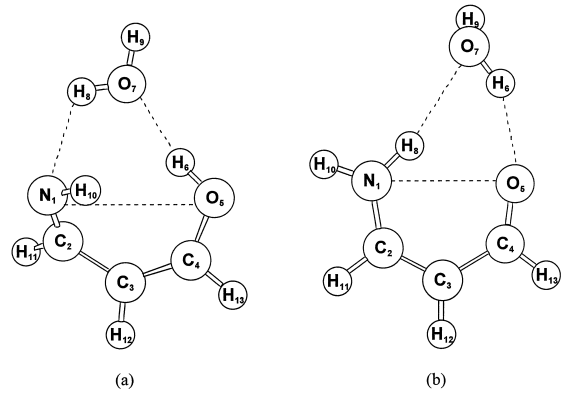

Fig. 5. The ground state optimized geometries of the (a) enol and (b) keto tautomers of the complex of 1-amino-3-propenal with water.

Table 5
Most relevant optimized geometrical parameters (Å and degrees) of the two tautomeric forms of the complex of 1-amino-3-propenal with a water molecule and the transition state that connects the two tautomers

	$r(N_1–C_2)$	$r(C_2–C_3)$	$r(C_3–C_4)$	$r(C_4–O_5)$	$r(N_1–H_8)$	$r(H_8–O_7)$	$r(O_7–H_6)$	$r(H_6–O_5)$	$r(O_5–N_1)$
enol									
S_0	1.264	1.480	1.336	1.331	2.322	0.948	1.930	0.955	3.253
S_0 [a]	*1.272*	*1.459*	*1.344*	*1.316*	*2.266*	*0.947*	*2.929*	*0.954*	*2.802*
$n\pi^*$	1.314	1.450	1.338	1.354	4.220	0.944	2.271	0.946	2.999
$\pi\pi^*$	1.332	1.414	1.453	1.287	1.715	0.977	1.400	1.000	3.324
TS									
S_0	1.317	1.410	1.403	1.254	1.403	1.112	1.043	1.422	2.979
$n\pi^*$	1.323	1.400	1.429	1.277	1.453	1.047	1.133	1.213	3.384
$\pi\pi^*$	1.332	1.428	1.452	1.271	1.295	1.143	1.211	1.135	3.361
keto									
S_0	1.335	1.364	1.444	1.213	1.000	2.220	0.950	2.004	2.892
$n\pi^*$	1.366	1.345	1.464	1.265	0.994	2.245	0.945	2.369	3.023
$\pi\pi^*$	1.336	1.447	1.434	1.248	1.005	2.298	0.951	1.974	2.789

[a] Values corresponding to the ground state planar enol conformer.

H-bond between H_6 and O_7 is substituted by a somewhat stronger H-bond between H_6 and N_1 [55] ($r(H_6–N_1) = 2.016$ Å). However, in this planar conformer the PT is not assisted by the water molecule bridge and so it is not expected to be much different from the PT analyzed in Section 3.1. For this reason, we have preferred to study the PT in the ground state for the nonplanar enol conformer which takes place through the water bridge. This notwithstanding, the excited states have been studied under C_S symmetry to avoid convergence problems.

Upon inspection of values in Tables 1 and 5, one can notice that the most important structural differences between 1-amino-3-propenal and its complex with water correspond to bond distances that change most during the PT process. The $r(N_1–H_8)$ and $r(O_7–H_6)$ bond distances in the enol form of the complex are larger than the $r(N_1–H_6)$ bond distance in the enol tautomer of 1-amino-3-propenal for the ground and the $n\pi^*$ states. This is especially remarkable in this latter case. The large $r(N_1–H_8)$ bond length in the $n\pi^*$ state is due to the fact that the water molecule of the enol complex in this state prefers to rotate to avoid Pauli repulsions rather than to form a weak H-bond between N_1 and H_8. Also, for the keto tautomer, the $r(H_8–O_7)$ and $r(H_6–O_5)$ bond distances are, in most cases, larger than the $r(O_5–H_6)$ bond length in 1-amino-3-propenal. Another remarkable difference corresponds to the $r(N_1–O_5)$ distance, which increases in the complex. The formation of an eight-membered ring between the water molecule and 1-amino-3-propenal forces the N_1 and the O_5 to move away.

Table 6 gathers the relative stability of the two tautomers and the energy barriers for the PT processes for the three electronic states analyzed. It is interesting to note that the relative stability between the two tautomers obtained by HF/CIS and MP2/CIS–MP2//HF/CIS level has not changed, the keto form being more stable than the enol tautomer.

Values in Table 6 indicate that the CIS energy barriers have increased considerably with respect to the energy barriers of 1-amino-3-propenal in all states. The $n\pi^*$ state has the largest barrier and the

Table 6
Energy difference (ΔE) between the two tautomeric forms of the complex of 1-amino-3-propenal with water and direct ($\Delta E_d^{\ddagger}$) and reverse ($\Delta E_r^{\ddagger}$) energy barriers for the proton transfer that transforms the enol to the keto form of this complex computed at HF/CIS and MP2/CIS–MP2//HF/CIS (in italics) level

	ΔE [a]	$\Delta E_d^{\ddagger}$ a	$\Delta E_r^{\ddagger}$ [a]
S_0	17.7	33.8	51.4
	16.4	*19.8*	*36.1*
$n\pi^*$	15.8	50.5	66.3
	27.3	*20.9*	*48.1*
$\pi\pi^*$	21.3	5.7	27.1
	22.1	*– 7.2*	*14.9*

[a] In kcal/mol.

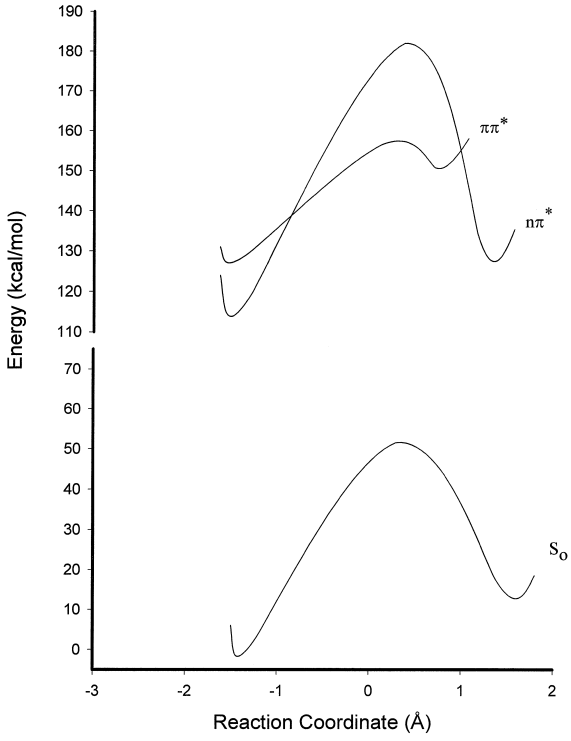

Fig. 6. Energy profiles for the proton transfer in the ground and excited states of the complex of 1-amino-3-propenal with water obtained by full geometry optimization in the ground state and imposing C_S symmetry in the geometry optimizations of the excited states. The reaction coordinate corresponds to the difference between N_1-H_8 and H_6-O_5 bond lengths. The zero energy value is taken as the energy of the keto tautomer in the ground state.

$\pi\pi^*$ state presents the lowest barrier as found for the 1-amino-3-propenal system. The increase of the energy barrier indicates that the PT in the complex is less favored than the PT in 1-amino-3-propenal. Although there are a number of systems in which the water-assisted mechanism favors the PT [49,80–86], the inhibition of the ESIPT process by intermolecular hydrogen-bonding interactions has also been reported [36,45,85,87]. In particular, the inhibition of the ESIPT process in ethanol solution has been observed for the *N*-phenylanthranilic acid [36], a system which contains the same OCCCN backbone as 1-amino-3-propenal. It has been recently reported that the PT energy barriers and H-bonds are lower and stronger, respectively, for the systems in which the PT takes place through a six-membered ring than for the systems with four- and five-membered rings in most electronic states [76]. This has been attributed to a reduction of the steric strain when the ring contains six atoms [76,86]. In agreement with this earlier study [76], our results show that the PT through an eight-membered ring of the complex of 1-amino-3-propenal with water is more difficult than the same PT through the six-membered ring present in 1-amino-3-propenal. Excepting the $\pi\pi^*$ state, the MP2/CIS–MP2//HF/CIS values follow the same trend even though the barriers are lower, indicating again that the CIS method overestimates the PT barriers.

The HF/CIS energy profiles for the ground state and the two lowest-lying singlet excited states along the PT reaction coordinate are depicted in Fig. 6. The lowest singlet excited states result from $\pi\pi^*$ and $n\pi^*$ excitations. It is noteworthy that the curves of the excited states in the complex are similar to those obtained for 1-amino-3-propenal. The double crossing between the two $n\pi^*$ and $\pi\pi^*$ excited states and the energetic order between the two excited states are also present in the complex with water. Although the energy barrier for the ESIPT in

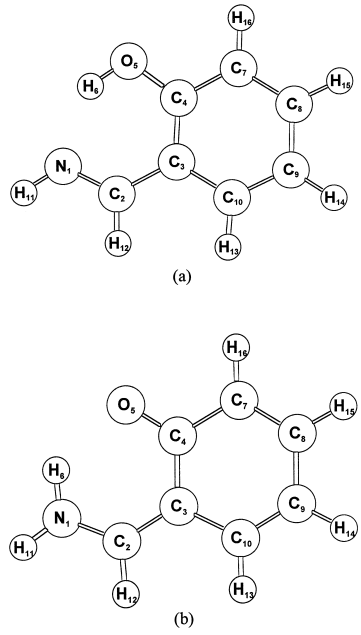

Fig. 7. The ground state optimized geometries of the (a) enol and (b) keto tautomers of salicylaldimine.

Table 7
Most relevant optimized geometrical parameters (Å and degrees) of the two tautomeric forms of salicylaldimine and the transition state that connects the two tautomers

	$r(C_3-C_4)$	$r(C_4-C_7)$	$r(C_7-C_8)$	$r(C_8-C_9)$	$r(C_9-C_{10})$	$r(C_{10}-C_3)$	$r(N_1-H_6)$	$r(O_5-H_6)$	$r(N_1-O_5)$	$\theta(N_1-H_6-O_5)$
enol										
S_0	1.405	1.397	1.382	1.397	1.380	1.400	1.869	0.957	2.696	143.0
$1\pi\pi^*$	1.494	1.404	1.395	1.417	1.401	1.401	1.660	0.991	2.560	148.9
$n\pi^*$	1.404	1.391	1.384	1.394	1.380	1.407	2.127	0.942	2.909	139.6
$2\pi\pi^*$	1.420	1.406	1.425	1.406	1.389	1.462	1.853	0.961	2.686	143.5
TS										
S_0	1.429	1.427	1.366	1.421	1.364	1.415	1.187	1.267	2.375	150.9
$1\pi\pi^*$	1.496	1.413	1.396	1.408	1.407	1.395	1.351	1.123	2.407	153.1
$n\pi^*$	1.432	1.417	1.369	1.417	1.362	1.423	1.202	1.191	2.317	150.9
$2\pi\pi^*$	1.432	1.419	1.422	1.408	1.377	1.473	1.196	1.266	2.387	151.7
keto										
S_0	1.465	1.462	1.348	1.447	1.346	1.443	1.002	1.930	2.665	127.9
$1\pi\pi^*$	1.494	1.432	1.404	1.386	1.423	1.391	1.001	1.988	2.707	126.7
$n\pi^*$	1.485	1.455	1.345	1.450	1.339	1.459	0.991	2.178	2.798	119.1
$2\pi\pi^*$	1.443	1.441	1.407	1.418	1.365	1.483	1.014	1.815	2.622	133.9

the $\pi\pi^*$ state is higher in the complex than in 1-amino-3-propenal, still it is low enough to allow a direct PT from the enol to the keto tautomer if the molecule does not decay to the $n\pi^*$ state through the conical intersection.

3.3. Salicylaldimine system

Fig. 7 illustrates the molecular structures of the two tautomers optimized in the ground state for salicylaldimine. It must be noted that despite these structures are planar in this state, the planarity is lost in the excited states, even though in minor degree than in 1-amino-3-propenal due to the presence of the ring. Remarkably, the structure of salicylaldimine is the same as the experimentally analyzed Schiff bases [25,37–39] like salicylidene methylamine (SMA), *N*-salicylidene aniline (SA), or *N*-salicylidene-1-naphthylamine (SN) by substituting H_{11} (Fig. 7) by methyl, benzyl or naphthyl substituents, respectively. For salicylaldimine the ground and the three lowest-lying singlet excited states have been examined.

Table 7 contains the geometrical parameters of salicylaldimine in its two tautomeric forms. According to a simple Lewis structure, the keto ring can be characterized by the presence of two double bonds ($C_7=C_8$, $C_9=C_{10}$), while the enol ring has a clear aromatic character. Upon inspection of the bond lengths in the ground state one can notice that despite the enol ring presents aromaticity, not all bonds are equivalent. The presence of the hydroxy and aminomethylidene substituents in the ring of the enol form leads to some π electronic charge localization into the C_3–C_4 bond. This, in turn, induces alternating bond distances in the ring of the enol form in the ground state, in a similar way to that found in the so-called Mills–Nixon effect [88–90].

Following the same scheme of Sections 3.1 and 3.2, let us now examine the energetic parameters presented in Table 8 for salicylaldimine. One of the most striking distinction between this system and the two systems already studied is the relative stability between the two tautomers. In all the states studied, excepting the $1\pi\pi^*$ state, the enol tautomer is more stable than the keto tautomer at the HF/CIS levels. In the ground state, the greater stability of the enol form, confirmed experimentally in neutral and polar nonprotic solvents for the SMA, SA, and SN species [25,37–39] is attributed to the aromaticity of its six-membered ring which is not present in the keto form.

Table 8
Energy difference (ΔE) between the two tautomeric forms of the salicylaldimine, and direct ($\Delta E_d^{\ddagger}$) and reverse ($\Delta E_r^{\ddagger}$) energy barriers for the proton transfer that transforms the enol to the keto form computed at HF/CIS and MP2/CIS–MP2//HF/CIS (in italics) level

	ΔE[a]	$\Delta E_d^{\ddagger}$[a]	$\Delta E_r^{\ddagger}$[a]
S_0	−6.8	14.4	7.7
	−8.9	*7.3*	*−1.6*
$1\pi\pi^*$	17.0	1.5	18.5
	20.3	*−7.1*	*13.2*
$n\pi^*$	−0.2	25.2	25.0
	27.8	*−25.6*	*2.3*
$2\pi\pi^*$	−7.1	12.2	5.0
	3.6	*−1.3*	*2.3*

[a] In kcal/mol.

The change in the relative stability of the enol and the keto forms when going from the ground state to the $1\pi\pi^*$ state has been experimentally reported in systems which have a similar structure to salicylaldimine like 2-(2′-hydroxyphenyl) benzoxazole [51], 2-(2′-hydroxyphenyl) benzimidazole [85,87] 2-(3′-hydroxy-2′-pyridyl) benzimidazole [43] and in the SMA, SA, and SN compounds [25,37–39]. The difference in vertical excitation energies between the enol and keto tautomers in the $1\pi\pi^*$ excited state is 15.9 kcal/mol at the HF/CIS level, favoring the keto tautomer. Therefore, the switch in the relative stability of the two tautomers in the $1\pi\pi^*$ state arises from the electronic redistribution after photoexcitation, and should already be explained by looking at the HOMO and LUMO orbitals in Fig. 8. As can be seen in this Figure, following the electronic excitation in the enol form there is a reduction of π bonding character on the C_3–C_4 bond, its double bond character being partially lost. In this way, the enol structure experiences a loss of aromaticity which diminishes its stability. This conclusion is reinforced by the geometrical parameters of the optimized structures in Table 7, which reveal that the most important changes in the bond lengths of adjacent atoms in the ring occur in the $1\pi\pi^*$ state. It is clear from these bond lengths that the six-membered ring of the enol form experiences an important

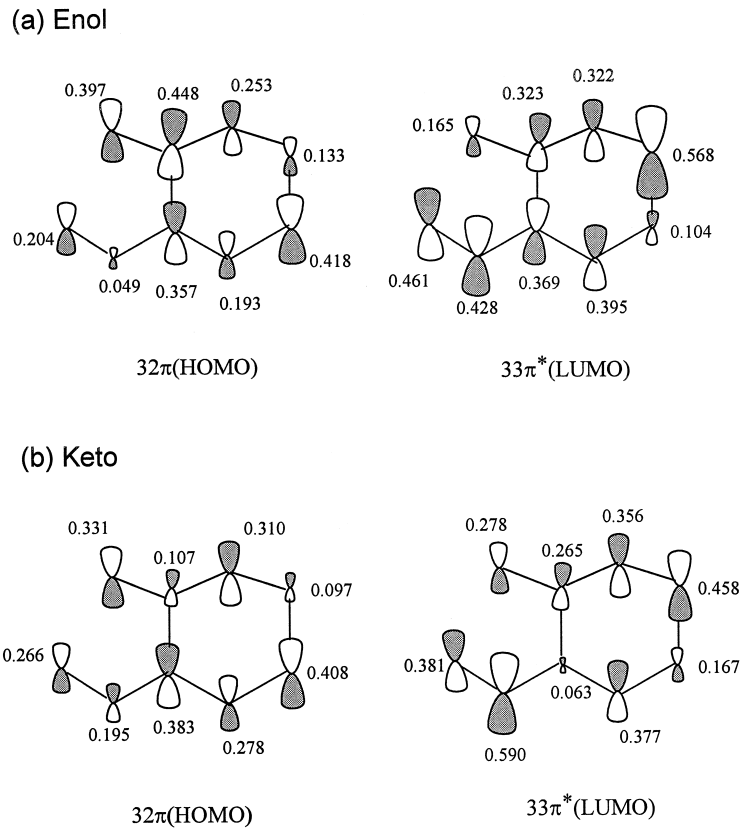

Fig. 8. Schematic diagram of the orbital structure of the HOMO and LUMO of the (a) enol and (b) keto tautomers of salicylaldimine. The numbers correspond to the value of the molecular orbital coefficient obtained from the square root of the sum of the squared coefficients of intervening atomic orbitals.

loss of its aromatic character, while the keto structure seems to experience a gain of aromaticity, which results in the reversal of the stability after $1\pi\pi^*$ photoexcitation. A similar effect was pointed out by Guallar et al. [40–42] in the analysis of the $1\pi\pi^*$ excitation in 2-(2′-hydroxyphenyl)-oxazole. Moreover, the $n\pi^*$ and $2\pi\pi^*$ excitations do not produce a significant loss of aromaticity as revealed by the C–C bond lengths of the ring in Table 7.

Another point that differentiates 1-amino-3-propenal and salicylaldimine is the values of the energy barriers. As expected from the large stability of the enol form, in all states, except the $1\pi\pi^*$ state, the direct barriers (from the enol to the keto tautomer) are larger than the reverse barriers at the HF/CIS level. The energy barriers for the direct and reverse PT in the ground state are low enough to allow the existence of an equilibrium between both tautomers at room temperature. The presence of this equilibrium has been confirmed experimentally for the SMA compound in acetonitrile solution [39]. MP2//HF method predicts also a greater stability for the enol form than the keto form in the ground state. However, the relative energy between the two tautomers computed by CIS–MP2//CIS method is reversed with respect to that found at the CIS level. The energy barriers predicted by CIS–MP2//CIS method are again negative, specially the energy barrier of the $n\pi^*$ state.

The HF/CIS energy profiles of the ground state and the three lowest-lying singlet excited states studied along the PT reaction coordinate are plotted in Fig. 9. The most important difference between 1-amino-3-propenal and salicylaldimine is the order of

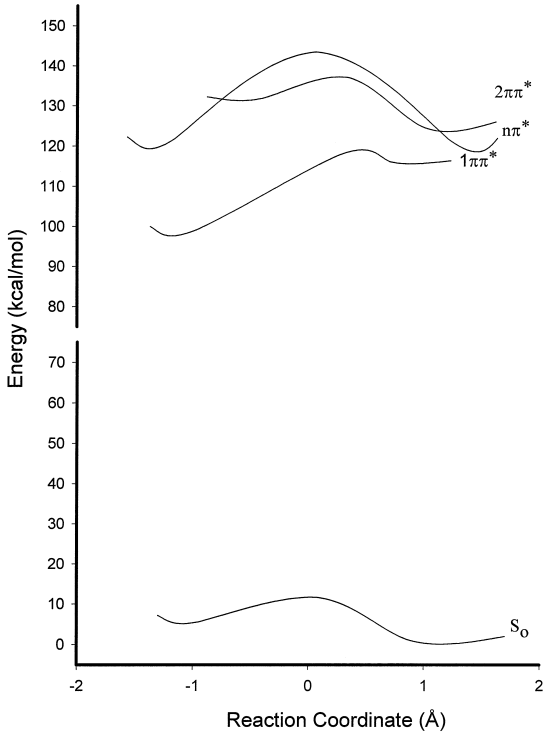

Fig. 9. Energy profiles for the proton transfer in the ground and excited states of salicylaldimine obtained by full geometry optimization in the ground state and imposing C_S symmetry in the geometry optimizations of the excited states. The reaction coordinate corresponds to the difference between N_1-H_6 and H_6-O_5 bond lengths. The zero energy value is taken as the energy of the enol tautomer in the ground state.

the two first excited states. Unlike 1-amino-3-propenal, the $1\pi\pi^*$ state has lower energy than the $n\pi^*$ state. The presence of the aromatic ring in salicylaldimine stabilizes the LUMO and destabilizes the HOMO with respect to the LUMO and HOMO of the more simple system [91]. Hence, the energy needed for $1\pi\pi^*$ excitation is lower in the more conjugated system. This was confirmed experimentally by Kownacki et al. [37] who showed that the extension of the π-electron system is followed by a red-shift of the absorption band. Further, the $n\pi^*$ state in this molecule does not play the role it does in 1-amino-3-propenal as a possible pathway for inhibition of the ESIPT process after $1\pi\pi^*$ excitation. Interestingly, excitation to the $2\pi\pi^*$ should not produce the strongly red-shifted fluorescence characteristic of the ESIPT processes. The same conclusions that those found here for salicylaldimine have been deduced from an experimental point of view for *o*-hydroxybenzaldehyde [92]. The important differences between 1-amino-3-propenal and salicylaldimine suggest that care must be taken in generalizing the results for models as small as 1-amino-3-propenal to the photochemistry of related larger compounds.

Remarkably, salicylaldimine presents a ground state and a $1\pi\pi^*$ excited state energy profiles along the PT reaction coordinate with the stability of the two tautomers reversed. Further, the energy profile of the $1\pi\pi^*$ state is almost barrierless along the PT coordinate. These are, precisely, the two necessary conditions for the ESIPT reaction to occur. In such a case, any photon emitted from the $1\pi\pi^*$ state in the keto form will be strongly red-shifted compared to any photon that excites the system from the ground to the $1\pi\pi^*$ state in the enol structure (our theoretical estimation of the red-shift is 13600 cm^{-1}). Experimentally, it has been observed in the SA and SN compounds [25,37] that electronic excitation within the absorption spectrum of the enol form produces a large red-shifted fluorescence in the emission spectrum of the keto form, and this confirms the presence of the ESIPT reaction predicted by the CIS methodology in a similar system such as salicylaldimine. It is worth mentioning that for the SMA system [39] the ESIPT has not been observed. However, this has been attributed to the fact that in this system there exists a more efficient route to the excited PT product which is the population of a photochromic transient in its ground state [39].

4. Conclusions

The potential energy surfaces of the ground and the two lowest-lying singlet excited states of 1-amino-3-propenal, the cyclic complex of 1-amino-3-propenal with water, and salicylaldimine have been investigated along the proton transfer reaction coordinate in order to discuss the changes induced by solvation and larger conjugation on the photochemistry of 1-amino-3-propenal.

The keto tautomer is preferred over the enol in the ground state and in the two first excited states of

1-amino-3-propenal. Following excitation to the $\pi\pi^*$ state of 1-amino-3-propenal, the system reacts through a low barrier to yield the keto tautomer and emitting the characteristic red-shifted fluorescence of the ESIPT processes, or conversely decays to the $n\pi^*$ state along the crossing between the two excited states and return to the ground state emitting slightly red-shifted fluorescence. The low barrier for the ESIPT process predicted by the CIS methodology for the $\pi\pi^*$ state is due to a deficiency of correlation in the CIS methodology, since a previous CASSCF study and the CIS–MP2//CIS results predict a barrierless PT for the same state. However, results have showed that qualitatively the CIS method describes correctly the ESIPT processes of 1-amino-3-propenal. The low barrier in the $\pi\pi^*$ state is consistent with the strong intramolecular H-bond found for this state.

The complex of 1-amino-3-propenal with water forms an eight-membered cycle which produces a considerably geometrical distortion of the molecule. The main consequence is that the proton transfer in the complex is less favored than in 1-amino-3-propenal for all states studied at the HF/CIS level.

It has been found that after adding a ring to the 1-amino-3-propenal system to yield the salicylaldimine molecule, the $1\pi\pi^*$ state is stabilized with respect to the $n\pi^*$ state, thus becoming the first excited state. The relative stability of the tautomers yielded by the HF/CIS method is reversed as compared to 1-amino-3-propenal, and the enol form is more stable than the keto tautomer, with the only exception of the $1\pi\pi^*$ state. In this state, the loss of aromaticity in the enol form after photoexcitation explains the change in the relative stability of the two tautomers. Hence, the photochemistry of salicylaldimine is completely different from that of 1-amino-3-propenal. Interestingly, the salicylaldimine system has the suitable ground and first excited state potential energy surfaces to be potentially useful in optical molecular memory systems.

Finally, the reduction of the energy barrier with the second-order perturbation correction in the ground and excited states shows that dynamic correlation is important to study the proton transfer reaction and indicates that the CIS method overestimates the barrier for the ESIPT processes. However, the large negative values of the CIS–MP2//CIS energy barriers obtained for some states lead to the conclusion that this method underestimates the energy barriers of the proton transfer processes.

Acknowledgements

This work has been funded through the Spanish DGICYT Project No. PB95-0762 and the European Union Project No. CI1*-CT93-0339. One of us (MF) thanks the Generalitat de Catalunya for financial help through CIRIT Project No. FI/96-05011.l. We acknowledge the Centre de Supercomputació de Catalunya (CESCA) for a generous allocation of computing time. We also thank Prof. O.N. Ventura for introducing us to this exciting topic.

References

[1] S.M. Ormson, R.G. Brown, Prog. React. Kin. 19 (1994) 45.
[2] D. Le Gourrierec, S.M. Ormson, R.G. Brown, Prog. React. Kin. 19 (1994) 221.
[3] A. Douhal, F. Lahmani, A.H. Zewail, Chem. Phys. 207 (1996) 477.
[4] A. Les, L. Adamowicz, J. Phys. Chem 94 (1990) 7021.
[5] A.L. Sobolewski, L. Adamowicz, J. Phys. Chem. 99 (1995) 14277.
[6] A.L. Sobolewski, L. Adamowicz, J. Chem. Phys. 102 (1995) 5708.
[7] A.L. Sobolewski, L. Adamowicz, Chem. Phys. Lett. 234 (1995) 94.
[8] M.A. Ríos, M.C. Ríos, J. Phys. Chem. 99 (1995) 12456.
[9] K.C. Hass, W.F. Schneider, C.M. Estévez, R.D. Bach, Chem. Phys. Lett. 263 (1996) 414.
[10] X. Duan, S. Scheiner, Chem. Phys. Lett. 204 (1993) 36.
[11] A.L. Sobolewski, W. Domcke, Chem. Phys. 184 (1994) 115.
[12] Z. Latajka, S. Scheiner, J. Phys. Chem. 96 (1992) 9764.
[13] K. Luth, S. Scheiner, J. Phys. Chem. 98 (1994) 3582.
[14] V. Barone, C. Adamo, J. Chem. Phys. 105 (1996) 11007.
[15] P.T. Chou, M. Chao, J.H. Clements, M.L. Martinez, Ch.P. Chang, Chem. Phys. Lett. 220 (1994) 229.
[16] A.L. Sobolewski, L. Adamowicz, Chem. Phys. 193 (1995) 67.
[17] V. Guallar, M. Moreno, J.M. Lluch, F. Amat-Guerri, A. Douhal, J. Phys. Chem. 100 (1996) 19789.
[18] Ch.M. Hadad, J.B. Foresman, K.B. Wiberg, J. Phys. Chem. 97 (1993) 4293.
[19] P.M. Felker, Wm.R. Lambert, A.H. Zewail, J. Chem. Phys. 77 (1982) 1603.
[20] J.L. Herek, S. Pedersen, L. Bañares, A.H. Zewail, J. Chem. Phys. 97 (1992) 9046.
[21] A. Douhal, F. Lahmani, A. Zehnacker-Rentien, Chem. Phys. 178 (1993) 493.

[22] N. Makri, W.H. Miller, J. Chem. Phys. 91 (1989) 4026.
[23] E. Bosch, M. Moreno, J.M. Lluch, Chem. Phys. 159 (1992) 99.
[24] P.F. Barbara, P.K. Walsh, L.E. Brus, J. Phys. Chem. 93 (1989) 29.
[25] A. Grabowska, K. Kownacki, J. Karpiuk, S. Dobrin, L. Kaczmarek, Chem. Phys. Lett. 267 (1997) 132.
[26] H.J. Heller, H.R. Blattmann, Pure Appl. Chem. 36 (1973) 141.
[27] D.L. Williams, A. Heller, J. Phys. Chem. 74 (1970) 4473.
[28] T. Werner, J. Phys. Chem. 83 (1979) 320.
[29] A.U. Khan, M. Kasha, Proc. Natl. Acad. Sci. USA 80 (1983) 1767.
[30] G.A. Brucker, T.C. Swinney, D.F. Kelley, J. Phys. Chem. 95 (1991) 3190.
[31] T. Nishiya, S. Yamauchi, N. Hirota, M. Baba, I. Hanazaki, J. Phys. Chem. 90 (1986) 5730.
[32] W. Frey, T. Elsaesser, Chem. Phys. Lett. 189 (1992) 565.
[33] M. Wiechmann, H. Port, F. Laermer, W. Frey, T. Elsaesser, Chem. Phys. Lett. 165 (1990) 28.
[34] Th. Arthen-Engeland, T. Bultmann, N.P. Ernsting, M.A. Rodríguez, W. Thiel, Chem. Phys. 163 (1992) 43.
[35] N.P. Ernsting, J. Phys. Chem. 89 (1985) 4932.
[36] F. Márquez, I. Zabala, F. Tomas, An. Quim. 91 (1995) 647.
[37] K. Kownacki, A. Mordzinski, R. Wilbrandt, A. Grabowska, Chem. Phys. Lett. 227 (1994) 270.
[38] K. Kownacki, L. Kaczmarek, A. Grabowska, Chem. Phys. Lett. 210 (1993) 373.
[39] A. Grabowska, K. Kownacki, L. Kaczmarek, Acta Phys. Pol. A. (Engl.) 88 (1995) 1081.
[40] I.A.Z. Al-Ansari, J. Lumin. 71 (1997) 83.
[41] S.K. Das, A. Bansal, S.K. Dogra, Bull. Chem. Soc. Jpn 70 (1997) 307.
[42] M. Mosquera, J.C. Penedo, M.C. Ríos-Rodríguez, F. Rodríguez-Prieto, J. Phys. Chem. 100 (1996) 5398.
[43] M. Mosquera, M.C. Ríos-Rodríguez, F. Rodríguez-Prieto, J. Phys. Chem. A. 101 (1997) 2766.
[44] E.L. Roberts, J. Dey, I.M. Warner, J. Phys. Chem. 100 (1996) 19681.
[45] G. Yang, F. Morlet-Savary, Z. Peng, S. Wu, J.P. Fouassier, Chem. Phys. Lett. 256 (1996) 536.
[46] A.L. Sobolewski, W. Domcke, Chem. Phys. Lett. 211 (1993) 82.
[47] S. Mitra, R. Das, S. Mukherjee, J. Mol. Liq. 68 (1996) 65.
[48] Y.R. Kim, J.T. Yardley, R.M. Hochstrasser, Chem. Phys. 136 (1989) 311.
[49] K. Das, D.S. English, J.W. Petrich, J. Am. Chem. Soc. 119 (1997) 2763.
[50] T. Nakayama, T. Hamana, S. Miki, K. Hamonouse, J. Chem. Soc., Faraday Trans. 92 (1996) 1473.
[51] R.M. Tarkka, S.A. Jenekhe, Chem. Phys. Lett. 260 (1996) 533.
[52] M.J. Frisch, G.W. Trucks, H.B. Schlegel, P.M.W. Gill, B.G. Johnson, M.A. Robb, J.R. Cheeseman, T.A. Keith, G.A. Petersson, J.A. Montgomery, K. Raghavachari, M.A. Al-Laham, V.G. Zakrewski, J.V. Ortiz, J.B. Foresman, J. Cioslowski, B. Stefanov, A. Nanayakkara, M. Challacombe, C.Y. Peng, P.Y. Ayala, W. Chen, M.W. Wong, J.L. Andrés, E.S. Replogle, R, Gomperts, R.L. Martin, D.J. Fox, J.S. Binkley, D.J. Defrees, J. Baker, J.J.P. Stewart, M. Head-Gordon, C. González, J.A. Pople, GAUSSIAN94 REVISION B.2, Gaussian, Pittsburgh, PA, 1995.
[53] J.B. Foresman, M. Head-Gordon, J.A. Pople, J. Phys. Chem. 96 (1992) 135.
[54] A.L. Sobolewski, L. Adamowicz, Chem. Phys. 213 (1996) 193.
[55] K. Luth, S. Scheiner, J. Phys. Chem. 99 (1995) 7352.
[56] T.H. Dunning Jr., P.J. Hay, in: H.F. Schaefer III (Ed.), Methods of Electronic Structure Theory (Plenum Press, New York 1977).
[57] R. Carbó, L. Leyda, M. Arnau, Int. J. Quantum Chem. 17 (1980) 1185.
[58] R. Carbó, B. Calabuig, Int. J. Quantum Chem. 42 (1992) 1681.
[59] R. Carbó, B. Calabuig, L. Vera, E. Besalú, Adv. Quantum Chem. 25 (1994) 253.
[60] E. Besalú, R. Carbó, J. Mestres, M. Solà, Topics Curr. Chem. Ser. 173 (1995) 31.
[61] E. Besalú, R. Carbó, in: R. Carbó (Ed.), Similarity and Reactivity: From Quantum Chemical to Phenomenological Approaches, Ch. 3 (Kluwer, Dordrecht, The Netherlands, 1995).
[62] M. Solà, J. Mestres, M. Duran, R. Carbó, J. Chem. Inf. Comput. Sci. 34 (1994) 1047.
[63] M. Solà, J. Mestres, M. Duran, R. Carbó, J. Am. Chem. Soc. 116 (1994) 5909.
[64] J. Mestres, M. Solà, M. Duran, R. Carbó, in: R. Carbó (Ed.), Molecular Similarity and Reactivity: From Quantum Chemical to Phenomenological Approaches (Kluwer, Dordrecht, The Netherlands, 1995) p. 89.
[65] J. Mestres, M. Solà, R. Carbó, F.J. Luque, M. Orozco, J. Phys. Chem. 100 (1996) 606.
[66] M. Solà, J. Mestres, R. Carbó, M. Duran, J. Chem. Phys. 104 (1996) 636.
[67] X. Fradera, Ll. Amat, M. Torrent, J. Mestres, P. Constans, E. Besalú, J. Martí, S. Simon, M. Lobato, J.M. Oliva, J.M. Luis, J.L. Andrés, M. Solà, R. Carbó, M. Duran, J. Mol. Struct. (THEOCHEM) 371 (1996) 171.
[68] N.C. Handy, H.F. Schaefer III, J. Chem. Phys. 81 (1984) 5031.
[69] K.B. Wiberg, C.M. Hadad, T.J. LePage, C.M. Breneman, M.J. Frisch, J. Phys. Chem. 96 (1992) 671.
[70] J. Mestres, M. Solà, E. Besalú, M. Duran, R. Carbó, MESSEM, Girona, CAT, 1993.
[71] E. Besalú, R. Carbó, M. Duran, J. Mestres, M. Solà, in: E. Clementi, G. Corongiu (Eds.), Methods and Techniques in Computational Chemistry (METTEC-95) (STEF, Cagliari 1995) p. 491.
[72] A. Douhal, Science 276 (1997) 221.
[73] M.C. Rovira, S. Scheiner, J. Phys. Chem. 99 (1995) 9854.
[74] C. Chudoba, E. Riedle, M. Pfeiffer, T. Elsaesser, Chem. Phys. Lett. 263 (1996) 622.
[75] M. Solà, J. Mestres, J.M. Oliva, M. Duran, R. Carbó, Int. J. Quantum Chem. 58 (1996) 361.

[76] S. Scheiner, T. Kar, M. Cuma, J. Phys. Chem. A 101 (1997) 5901.
[77] M. Solà, J. Mestres, R. Carbó, M. Duran, J. Chem. Phys. 104 (1996) 636.
[78] M. Forés, L. Adamowicz, submitted for publication.
[79] F. Bernardi, M. Olivucci, M.A. Robb, Chem. Soc. Rev. (1996) 321.
[80] M. Solà, A. Lledós, M. Duran, J. Bertrán, J. Am. Chem. Soc. 114 (1992) 869.
[81] J.Y. Liang, W.N. Lipscomb, Int. J. Quantum Chem. 36 (1989) 299.
[82] A. Lledós, J. Bertrán, J. Mol. Struct. (THEOCHEM) 120 (1985) 73.
[83] O. Ventura, A. Lledós, R. Bonaccorsi, J. Bertrán, J. Tomasi, Theor. Chim. Acta 72 (1987) 175.
[84] P. Ruelle, J. Am. Chem. Soc. 109 (1987) 1722.
[85] J. Herbich, J. Dobkowski, R.P. Thummel, V. Hegde, J. Waluk, J. Phys. Chem. A. 101 (1997) 5839.
[86] M.S. Gordon, J. Phys. Chem. 100 (1996) 3974.
[87] E.L. Roberts, J. Dey, I.M. Warner, J. Phys. Chem. A 101 (1997) 5296.
[88] W.M. Mills, I.G. Nixon, J. Chem. Soc. (1930) 2510.
[89] P.C. Hiberty, G. Ohanessian, F. Delbecq, J. Am. Chem. Soc. 107 (1985) 3095.
[90] B.M. Trost, G.M. Bright, C. Frihart, D. Britelli, J. Am. Chem. Soc. 93 (1971) 737.
[91] M. Solà, J. Mestres, M. Duran, J. Phys. Chem. 99 (1995) 10752.
[92] S. Nagaoka, Y. Shinde, K. Mukai, U. Nagashima, J. Phys. Chem. A 101 (1997) 3061.